

# Detection of Polycyclic Aromatic Hydrocarbons in High Organic Carbon Ultrafine Particle Extracts by Electrospray Ionization Ultrahigh-Resolution Mass Spectrometry

Eric Schneider, Barbara Giocastro, Christopher P. R ger,\* Thomas W. Adam, and Ralf Zimmermann





Cite This: <https://doi.org/10.1021/jasms.2c00163>



Read Online

ACCESS |

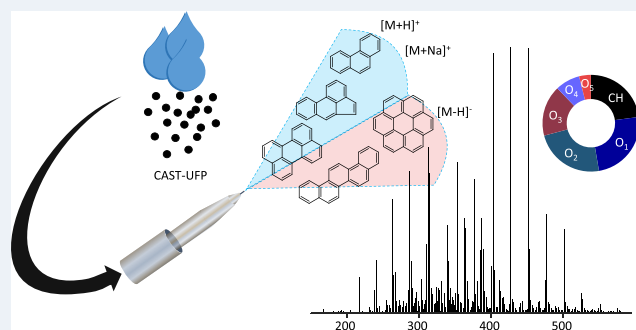
 Metrics & More

 Article Recommendations

 Supporting Information

**ABSTRACT:** The detection of polycyclic aromatic hydrocarbons (PAHs) by electrospray ionization (ESI) without additional reagents or targeted setup changes to the ionization source was observed in ultrafine particle (UFP) extracts, with high organic carbon (OC) concentrations, generated by a combustion aerosol standard (CAST) soot generator. Particulate matter (PM) was collected on filters, extracted with methanol, and analyzed by ESI Fourier-transform ion cyclotron resonance mass spectrometry (FT-ICR MS). Next to oxygen-containing species, pure hydrocarbons were found to be one of the most abundant compound classes, detected as  $[M + Na]^+$  or  $[M + H]^+$  in ESI+ and mostly as  $[M - H]^-$  in ESI-. The assigned hydrocarbon elemental compositions

are identified as PAHs due to their high aromaticity index (AI > 0.67) and were additionally confirmed by MS/MS experiments as well as laser desorption ionization (LDI). Thus, despite the relatively low polarity, PAHs have to be considered in the molecular attribution of these model aerosols and/or fresh emissions with low salt content investigated by ESI.



## INTRODUCTION

Polycyclic aromatic hydrocarbons (PAHs) are frequently emitted by incomplete combustion processes of most carbonaceous fuel types, e.g., fossil fuel, biomass, and are therefore frequently found as pollutants in the environment. Additionally, PAHs induce strong toxicological effects, including carcinogenic effects through reactive metabolites, which are also a source of reactive oxygen species (ROS), which induce oxidative stress.<sup>1,2</sup> Therefore, when analyzing the chemical composition of particulate matter (PM), the identification of PAHs is of high interest. Anthropogenic emission of particulate matter from industrial or urban sources like engines or biomass burning, is responsible for global adverse health effects.<sup>3</sup> Ultrafine particles (UFP, aerodynamic diameter  $\leq 100$  nm) are of particular interest due to their high particle number concentrations, as well as high capability to adsorb toxic compounds to their surface and the ability to transport these compounds deep into the respiratory system.<sup>1,4</sup>

Electrospray ionization (ESI) is a frequently applied ionization technique for the analysis of liquid aerosol extracts, due to its softness and sensitive ionization of polar compounds (e.g., oxygen-containing functionalities), which are frequently found in aerosol samples.<sup>5,6</sup> Nonpolar compounds like PAHs are usually not observed under standard ESI conditions, due to their poor ionization efficiency and ionization suppression from more readily ionized polar molecules.<sup>7</sup> For nonpolar compounds, atmospheric pressure photoionization (APPI) or

laser desorption ionization (UV-LDI) have recently been established as comprehensive ionization techniques, but with the drawback of a lower sensitivity for highly oxygenated compounds.<sup>8</sup>

The unexpected detection of PAHs in addition to a range of oxygenated species under standard ESI conditions of a model PM extract is reported here, representing fresh high organic carbon (OC) soot emissions as well as similar artificially generated aerosols. With detectability of PAHs within the fresh low-polar PM, misattribution and missing their contribution, also in ESI spectra, will be addressed in this short communication.

## EXPERIMENTAL SECTION

**Sample Preparation.** A combustion aerosol standard (CAST) soot generator operated with propane was used to generate high organic carbon ultrafine particles. PM was collected on quartz fiber filters (47 mm diameter), and one-half of each filter was placed in a prebaked extraction vial and

**Received:** June 13, 2022

**Revised:** September 28, 2022

**Accepted:** September 30, 2022

65 then extracted with 5 mL of methanol (LC-MS grade) under  
66 shaking for 30 min. The extracts were filtered through a 0.2  $\mu\text{m}$   
67 PTFE membrane (Sartorius, Goettingen, Germany) in a  
68 stainless-steel filter holder via a glass syringe and stored at  
69  $-25\text{ }^\circ\text{C}$  until further analysis.

70 **ESI/LDI-FTICR-MS Measurements.** Ultrahigh-resolution  
71 FT-ICR-MS measurements were carried out on a Solarix  
72 (Bruker Daltonik, Bremen, Germany) equipped with a 7 T  
73 superconducting magnet. The samples were analyzed in  
74 positive and negative ionization mode with a direct-infusion  
75 ESI ion source setup (Bruker Daltonik, API Ion Source). The  
76 following ionization parameter were selected for positive/  
77 negative ion mode (ESI  $\pm$ ) respectively: capillary voltage  
78  $-3.3/3.7\text{ kV}$ , drying gas temperature  $180\text{ }^\circ\text{C}$ , drying gas flow  
79 rate  $4.0\text{ L/min}$ , nebulizer gas flow rate  $1.4\text{ bar}$ , quadrupole  
80 mass  $m/z\ 120$ , and syringe flow rate  $300\ \mu\text{L/h}$ . 200/300 scans  
81 were collected for each measurement with a  $1.96\text{ s}$  (4M)  
82 transient and a resulting resolving power of  $>310000$  at  $m/z$   
83  $400$ .

84 For laser desorption/ionization (UV-LDI) experiments, 20  
85  $\mu\text{L}$  of the respective extracts was spiked on multiple spots of  
86 the LDI-target-plate, and the solvent was allowed to evaporate.  
87 The number of laser shots was set to 100, with a laser  
88 frequency of  $500\text{ Hz}$  and a laser power of  $25\%$ .

89 **Data Analysis.** Raw data were peak picked (cutoff:  $S/N =$   
90  $9$ ) and exported with Bruker Data Analysis 5.1 (Bruker  
91 Daltonik, Bremen, Germany). The exported mass spectra were  
92 processed by self-written MATLAB algorithms and routines  
93 combined in a graphical user interface named CERES  
94 Processing. After careful investigation and consideration of  
95 reasonable attribution boundaries, we deployed the following  
96 restrictions for elemental composition assignment in the range  
97 of  $120\text{--}1000\text{ Da}$  with an assignment error of  $<1\text{ ppm}$ :  
98  $\text{C}_c\text{H}_h\text{O}_o\text{Na}_{na}$ ;  $6 \leq c \leq 100$ ,  $6 \leq h \leq 200$ ,  $o \leq 5$ ,  $na \leq 1$ .  
99 Additional restrictions were applied for the H/C ratio:  $0.4\text{--}$   
100  $2.4$ , O/C ratio:  $0\text{--}1.4$ , and double bond equivalents: DBE  $0\text{--}$   
101  $50$ . DBE and aromaticity index (AI) calculations are described  
102 in the Supporting Information.<sup>9</sup> Blank filters were processed  
103 according to the same procedure and used for blank correction.  
104 For ESI measurements, data from triplicate filter samples  
105 generated from the repetition of the same experimental CAST  
106 conditions were combined for data evaluation, including only  
107 sum formulas found in at least two measurements.

## 108 ■ RESULTS AND DISCUSSION

109 Both ESI polarities display a high molecular complexity of  
110 elemental compositions within the  $\text{CHO}_x$  ( $x = 0\text{--}5$ )  
111 compound class (Figures 1 and S1), mainly in the range of  
112  $m/z\ 150\text{--}800$  (ESI+, 900 formulas) or  $m/z\ 150\text{--}600$  (ESI-,  
113 500 formulas). Oxygenated species are the dominant group in  
114 both polarities, as would be expected for ionization with ESI,  
115 which is sensitive to polar compounds (i.e., oxygen-containing  
116 functional groups).<sup>5</sup> While in ESI- mostly  $[\text{M} - \text{H}]^-$  ions are  
117 observed (some  $[\text{M}]^\bullet$ ), in ESI+  $[\text{M} + \text{Na}]^+$  adducts are  
118 most common, with only minor contributions of  $[\text{M} + \text{H}]^+$   
119 ions.

120 Remarkably, it was also possible to detect high numbers of  
121 signals containing only CH (ESI  $\pm$ : 180/120 sum formulas,  
122 counting  $\text{Na}^+$  and  $\text{H}^+$  adducts each). The CH formulas contain  
123 an average of  $32/29$  carbon atoms and show exclusively  
124 particularly high DBE values in a narrow range ( $\overline{\text{DBE}}_{\text{ESI}^+} = 22$   
125  $\pm 11$ ,  $\overline{\text{DBE}}_{\text{ESI}^-} = 21 \pm 8$ , Figure S2), as well as high aromaticity

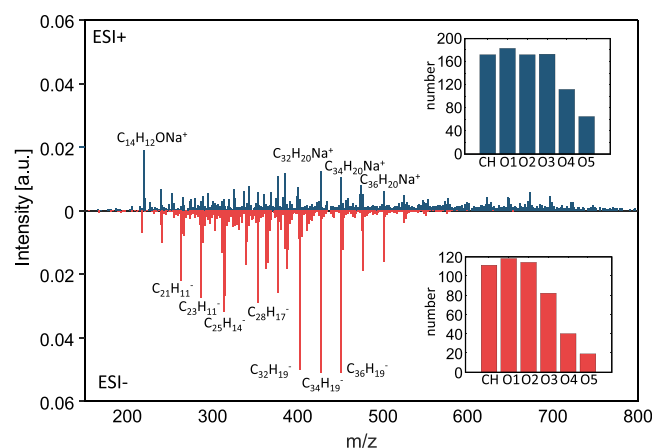


**Figure 1.** ESI-FTICR-MS mass spectra of intensities normalized to the total sum of intensity with ESI+ data in blue (top) and ESI- data in red (bottom). Prominent peaks are labeled with their assigned elemental composition. Compound class formula number distribution of ESI $\pm$  as insets (right).

indices of  $0.66/0.74$  in ESI $\pm$ , which suggests the classification 126  
as condensed polycyclic aromatic hydrocarbons (PAHs) from 127  
a pyrogenic process. This is stressed by the distribution 128  
displayed in Figure 2, which shows predominantly AI values 129  $\Omega$

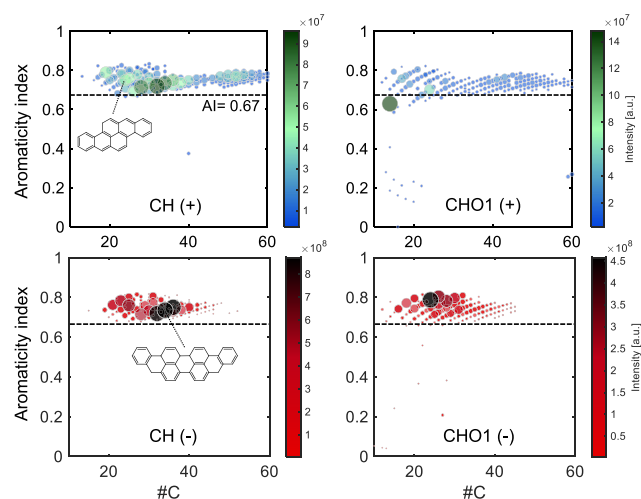


**Figure 2.** Aromaticity index versus carbon number (#C) plot of CH and  $\text{CHO}_1$  compound classes in ESI $\pm$  with exemplary molecular structures. AI  $> 0.67$  indicated by a dotted line to highlight region of condensed aromatic molecules.

larger than the frequently applied limit for condensed aromatic 130  
structures of AI  $> 0.67$ .<sup>9</sup> Oxygen-containing molecules 131  
observed here show similar properties regarding their 132  
aromaticity. This leads to the conclusion that these species 133  
are formed through the partial oxidation of aromatic core 134  
molecules, which are precursors in soot formation,<sup>10</sup> during the 135  
propane combustion process in the CAST or shortly afterward 136  
in the still-hot exhaust area. Consequently, this model aerosol 137  
serves as an example for other artificially generated PM or fresh 138  
soot emissions, e.g., from coal combustion or malfunctioning 139  
engines. 140

As ESI is sensitive to the detection of even low 141  
concentrations of polar compounds, it is possible to detect 142

143 these CHO<sub>1–5</sub> species that are not accessible by, e.g., gas  
144 chromatography. In most cases, CH species are not ionized by  
145 direct-infusion ESI due to their poor ionization efficiency  
146 based on the lack of polar moieties and consequently strong  
147 matrix effects/ion suppression.<sup>11</sup> To overcome this limitation,  
148 derivatization with tropylium ions or cationization with Ag(I)  
149 can be applied to improve the detection of PAHs, e.g., in LC-  
150 ESI-MS, through the formation of adduct ions which are  
151 subsequently fragmented by collision induced dissociation  
152 (CID) to generate radical molecule cations.<sup>12–15</sup> Another way  
153 of generating radical cations is the application of chemical  
154 electron transfer reagents (e.g., oxidants) like trifluoroacetic  
155 acid (TFA) or SbF<sub>5</sub>.<sup>16</sup>

156 Other reports of PAH ionization by ESI, e.g., from heavy  
157 crude oil asphaltene,<sup>17</sup> Arabian mix vacuum residue,<sup>7,18</sup> coal  
158 fire sponge extracts,<sup>19</sup> or individual PAHs,<sup>11,20</sup> describe the  
159 formation of protonated molecule-ions by addition of acid to  
160 the solvents or the formation of radical cations by abstraction  
161 of an electron at the surface of the ESI spray capillary,<sup>21</sup> but no  
162 dominant PAH-sodium-adduct formation.

163 Additionally, to the best of our knowledge, the detection of  
164 PAHs by ESI<sup>–</sup> has not been reported, particularly not for this  
165 PM matrix. In the case of this ultrafine particle model aerosol  
166 with a high share of organic carbon (OC, 0.02 mg C/m<sup>3</sup>),  
167 PAHs are found to be the main fraction of OC with  
168 concentrations of 3–6 ring PAHs in the range of 10–700  
169 ng/m<sup>3</sup> (PM) and 1–20 ppb (extract, EPA PAH, Table S1).  
170 The high concentrations of PAHs in combination with low  
171 concentrations of polar compounds, that would compete for  
172 charges during the ionization process of ESI and therefore  
173 suppress the ionization of PAH, seem to enable the ionization  
174 of CH species as adduct ions in ESI<sup>+</sup>.

175 The observation of CH species with ESI from the methanol  
176 filter extracts was also confirmed by LDI-FTICR-MS measure-  
177 ments, (Figure S3) that identified at least 35 CH compounds  
178 matching the ESI data. UV-LDI is a selective method for the  
179 detection of PAHs up to high *m/z* due to their suitable light-  
180 absorbing properties.<sup>8</sup> Additionally, ESI-FTICR-MS/MS ex-  
181 periments of selected peaks by CID provide supporting  
182 structural information (Figures 3 and S4). For example, the  
183 MS/MS spectrum of C<sub>24</sub>H<sub>12</sub>Na<sup>+</sup> (measured *m/z*: 323.08304)  
184 shows only three fragment signals, which match possible  
185 fragment-sodium adducts of condensed polycyclic aromatic

ring structures comparable to coronene and its structural  
isomers. As expected from condensed aromatic ring structures,  
the relative intensity of fragments is low. Furthermore, when  
increasing the CID energy, the intensity of the fragment ions is  
not increased (Figure S5). At a higher CID energy, the charge  
carrying sodium is abstracted from the molecule, before more  
pronounced fragmentation of C–C bonds occurs. Therefore,  
the detection of elemental compositions by both ionization  
techniques creates high certainty for the assignment of CH  
compounds in ESI as PAHs. When comparing ESI data from  
positive and negative ionization mode, it is apparent that ESI<sup>+</sup>  
is better suited for the ionization of PAHs, as more compounds  
are detected, especially for *m/z* > 500. Still, there is a  
significant overlap of compounds found in both ionization  
modes matching multiring pyrogenic soot precursors (Figure  
S6), e.g. C<sub>32</sub>H<sub>20</sub>, C<sub>34</sub>H<sub>20</sub>, C<sub>36</sub>H<sub>20</sub>.

Aromatic structures can stabilize a negative charge in  
molecules after deprotonation as the number of  $\pi$ -electrons,  
forming the delocalized aromatic  $\pi$ -system.<sup>22</sup> For planar  
aromatic CH compounds without electron-donating non-  
aromatic C–H bonds, which may be deprotonated due to  
higher acidity, [M]<sup>•–</sup> are also observed. As PAHs have a  
comparably high electron affinity, they can stabilize an electron  
by electron attachment, as was previously discussed for  
negative LDI of a PAH rich asphaltene fraction.<sup>23</sup>

In ESI<sup>+</sup>, mostly sodium adducts of PAHs are observed. This  
behavior could be explained by the ability of polycyclic  
aromatic ring systems to form adduct bonds with sodium ions  
(cation- $\pi$  interaction), that are relatively stable and con-  
sequently able to withstand the ion transfer plus even some  
CID voltage (Figure S5). The sodium- $\pi$  interaction of PAHs in  
ESI may be a point of future work, to increase the  
understanding of this effect, especially regarding the relevance  
of PAHs in environmental samples, such as aerosols.

## CONCLUSION

In summary, polycyclic aromatic hydrocarbons were detected  
up to *m/z* 800 by ionization with ESI in negative and positive  
ionization modes, in polar extracts of high organic carbon  
ultrafine particles generated by a CAST. PAHs in ESI<sup>+</sup> were  
mainly detected as sodium adducts, while predominately  
deprotonation was observed in ESI<sup>–</sup>. The identification of  
PAHs was also confirmed by LDI and ESI-MS/MS experi-  
ments. High concentrations of PAHs from the artificial, but not  
unrealistic, aerosol sample enable the ionization of nonpolar  
PAHs without any derivatization or acidification, although  
polar species (CHO<sub>*x*</sub>) are also abundant. Future experiments  
investigating similar, high organic carbon aerosols need to be  
open for the possibility of the detection of nonpolar CH  
compounds with ESI in both ionization modes to avoid errors  
in formula assignments and data interpretation.

## ASSOCIATED CONTENT

### Supporting Information

The Supporting Information is available free of charge at  
<https://pubs.acs.org/doi/10.1021/jasms.2c00163>.

Additional mass spectrometric data and GC-MS results  
(PDF)

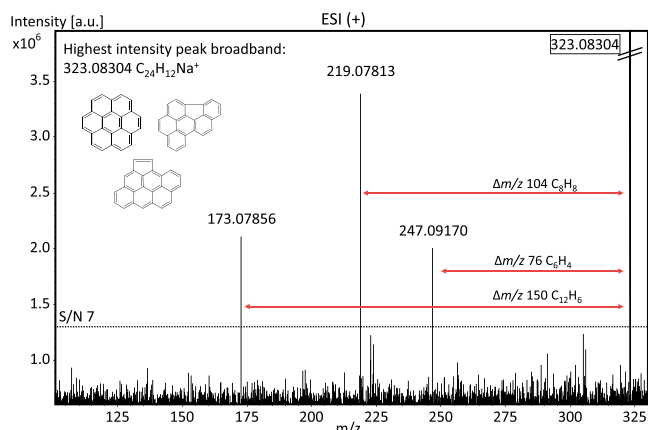



Figure 3. CID-MS/MS-FTICR spectrum of nominal mass *m/z* 323 in ESI<sup>+</sup> (CID = 5 V). Elemental composition assigned to molecular ion C<sub>24</sub>H<sub>12</sub>Na<sup>+</sup> with potential isomeric structures displayed.



## 242 ■ AUTHOR INFORMATION

## 243 Corresponding Author

244 Christopher P. Rüger – Joint Mass Spectrometry Centre  
245 (JMSC), Chair of Analytical Chemistry, University Rostock,  
246 18059 Rostock, Germany; Department Life, Light & Matter  
247 (LLM), University of Rostock, 18059 Rostock, Germany;  
248  [orcid.org/0000-0001-9634-9239](https://orcid.org/0000-0001-9634-9239);  
249 Email: [christopher.rueger@uni-rostock.de](mailto:christopher.rueger@uni-rostock.de)

## 250 Authors

251 Eric Schneider – Joint Mass Spectrometry Centre (JMSC),  
252 Chair of Analytical Chemistry, University Rostock, 18059  
253 Rostock, Germany; Department Life, Light & Matter (LLM),  
254 University of Rostock, 18059 Rostock, Germany

255 Barbara Giocastro – Institute of Chemistry and  
256 Environmental Engineering, University of the Bundeswehr  
257 Munich, 85579 Neubiberg, Germany

258 Thomas W. Adam – Institute of Chemistry and  
259 Environmental Engineering, University of the Bundeswehr  
260 Munich, 85579 Neubiberg, Germany; Joint Mass  
261 Spectrometry Center (JMSC) at Comprehensive Molecular  
262 Analytics (CMA), Helmholtz Munich, 85764 Neuherberg,  
263 Germany

264 Ralf Zimmermann – Joint Mass Spectrometry Centre  
265 (JMSC), Chair of Analytical Chemistry, University Rostock,  
266 18059 Rostock, Germany; Department Life, Light & Matter  
267 (LLM), University of Rostock, 18059 Rostock, Germany;  
268 Joint Mass Spectrometry Center (JMSC) at Comprehensive  
269 Molecular Analytics (CMA), Helmholtz Munich, 85764  
270 Neuherberg, Germany

271 Complete contact information is available at:

272 <https://pubs.acs.org/10.1021/jasms.2c00163>

## 273 Notes

274 The authors declare no competing financial interest.

## 275 ■ ACKNOWLEDGMENTS

276 This work was supported by the Horizon 2020 EU FT-ICR-  
277 MS project under Grant ID: 731077 and BAYUFP TLK01L-  
278 77228.

## 279 ■ REFERENCES

280 (1) Li, N.; Georas, S.; Alexis, N.; Fritz, P.; Xia, T.; Williams, M. A.;  
281 Horner, E.; Nel, A. A work group report on ultrafine particles  
282 (American Academy of Allergy, Asthma & Immunology): Why  
283 ambient ultrafine and engineered nanoparticles should receive special  
284 attention for possible adverse health outcomes in human subjects.  
285 *Journal of allergy and clinical immunology* **2016**, *138* (2), 386–396.  
286 (2) Stading, R.; Gastelum, G.; Chu, C.; Jiang, W.; Moorthy, B.  
287 Molecular mechanisms of pulmonary carcinogenesis by polycyclic  
288 aromatic hydrocarbons (PAHs): Implications for human lung cancer.  
289 *Seminars in cancer biology* **2021**, *76*, 3–16.  
290 (3) Di, Q.; Wang, Y.; Zanobetti, A.; Wang, Y.; Koutrakis, P.; Choirat,  
291 C.; Dominici, F.; Schwartz, J. D. Air Pollution and Mortality in the  
292 Medicare Population. *New England journal of medicine* **2017**, *376*  
293 (26), 2513–2522.  
294 (4) Juarez Facio, A. T.; Yon, J.; Corbière, C.; Rogez-Florent, T.;  
295 Castilla, C.; Lavanant, H.; Mignot, M.; Devouge-Boyer, C.; Logie, C.;  
296 Chevalier, L.; Vaugeois, J.-M.; Monteil, C. Toxicological impact of  
297 organic ultrafine particles (UFPs) in human bronchial epithelial  
298 BEAS-2B cells at air-liquid interface. *Toxicology in vitro* **2022**, *78*,  
299 105258.  
300 (5) Song, J.; Li, M.; Fan, X.; Zou, C.; Zhu, M.; Jiang, B.; Yu, Z.; Jia,  
301 W.; Liao, Y.; Peng, P. Molecular Characterization of Water- and

Methanol-Soluble Organic Compounds Emitted from Residential  
302 Coal Combustion Using Ultrahigh-Resolution Electrospray Ionization  
303 Fourier Transform Ion Cyclotron Resonance Mass Spectrometry.  
304 *Environ. Sci. Technol.* **2019**, *53* (23), 13607–13617. 305

(6) Schneider, E.; Czech, H.; Popovicheva, O.; Lüttdke, H.; Schnelle-  
306 Kreis, J.; Khodzher, T.; Rüger, C. P.; Zimmermann, R. Molecular  
307 Characterization of Water-Soluble Aerosol Particle Extracts by  
308 Ultrahigh-Resolution Mass Spectrometry: Observation of Industrial  
309 Emissions and an Atmospherically Aged Wildfire Plume at Lake  
310 Baikal. *ACS Earth Space Chem.* **2022**, *6* (4), 1095–1107. 311

(7) Miyabayashi, K.; Naito, Y.; Tsujimoto, K.; Miyake, M. Structure  
312 characterization of polyaromatic hydrocarbons in Arabian mix vacuum  
313 residue by electrospray ionization Fourier transform ion cyclotron  
314 resonance mass spectrometry. *Int. J. Mass Spectrom.* **2004**, *235* (1),  
315 49–57. 316

(8) Apicella, B.; Carpentieri, A.; Alfè, M.; Barbella, R.; Tregrossi, A.;  
317 Pucci, P.; Ciajolo, A. Mass spectrometric analysis of large PAH in a  
318 fuel-rich ethylene flame. *Proc. Combust. Inst.* **2007**, *31* (1), 547–553. 319

(9) Koch, B. P.; Dittmar, T. From mass to structure: an aromaticity  
320 index for high-resolution mass data of natural organic matter. *Rapid*  
321 *Commun. Mass Spectrom.* **2006**, *20* (5), 926–932. 322

(10) Haynes, B. S.; Wagner, H. Soot formation. *Prog. Energy*  
323 *Combust. Sci.* **1981**, *7* (4), 229–273. 324

(11) Hettiyadura, A. P. S.; Laskin, A. Quantitative analysis of  
325 polycyclic aromatic hydrocarbons using high-performance liquid  
326 chromatography-photodiode array-high-resolution mass spectrometric  
327 detection platform coupled to electrospray and atmospheric pressure  
328 photoionization sources. *J Mass Spectrom.* **2021**, *57* (2), e4804. 329

(12) Takino, M.; Daishima, S.; Yamaguchi, K.; Nakahara, T.  
330 Determination of polycyclic aromatic hydrocarbons by liquid  
331 chromatography–electrospray ionization mass spectrometry using  
332 silver nitrate as a post-column reagent. *J. Chromatogr. A* **2001**, *928*  
333 (1), 53–61. 334

(13) Lien, G.-W.; Chen, C.-Y.; Wu, C.-F. Analysis of polycyclic  
335 aromatic hydrocarbons by liquid chromatography/tandem mass  
336 spectrometry using atmospheric pressure chemical ionization or  
337 electrospray ionization with tropylium post-column derivatization.  
338 *Rapid Commun. Mass Spectrom.* **2007**, *21* (22), 3694–3700. 339

(14) Ghislain, T.; Faure, P.; Michels, R. Detection and monitoring of  
340 PAH and oxy-PAHs by high resolution mass spectrometry:  
341 comparison of ESI, APCI and APPI source detection. *J. Am. Soc.*  
342 *Mass Spectrom.* **2012**, *23* (3), 530–536. 343

(15) Maziarz, E. P., III; Baker, G. A.; Wood, T. D. Electrospray  
344 ionization Fourier transform mass spectrometry of polycyclic aromatic  
345 hydrocarbons using silver(I)-mediated ionization. *Can. J. Chem.* **2005**,  
346 *83* (11), 1871–1877. 347

(16) van Berkel, G. J.; Asano, K. G. Chemical Derivatization for  
348 Electrospray Ionization Mass Spectrometry. 2. Aromatic and Highly  
349 Conjugated Molecules. *Anal. Chem.* **1994**, *66* (13), 2096–2102. 350

(17) Molnár Gúricza, L.; Schrader, W. Electrospray ionization for  
351 determination of non-polar polyaromatic hydrocarbons and poly-  
352 aromatic heterocycles in heavy crude oil asphaltene. *J Mass Spectrom.*  
353 **2015**, *50* (3), 549–557. 354

(18) Miyabayashi, K.; Suzuki, K.; Teranishi, T.; Naito, Y.;  
355 Tsujimoto, K.; Miyake, M. Molecular Formula Determination of  
356 Constituents in Arabian Mix Vacuum Residue by Electrospray  
357 Ionization Fourier Transform Ion Cyclotron Resonance Mass  
358 Spectrometry. *Chem. Lett.* **2000**, *29* (2), 172–173. 359

(19) Xu, D.; Liang, Y.; Hong, X.; Liang, M.; Liang, H. Specification  
360 of complex-PAHs in coal fire sponges (CFS) by high-resolution mass  
361 spectrometry with electrospray ionization. *Environ. Sci. Pollut. Res.*  
362 **2021**, DOI: [10.1007/s11356-021-12929-3](https://doi.org/10.1007/s11356-021-12929-3). 363

(20) Cha, E.; Jeong, E. S.; Han, S. B.; Cha, S.; Son, J.; Kim, S.; Oh,  
364 H. B.; Lee, J. Ionization of Gas-Phase Polycyclic Aromatic  
365 Hydrocarbons in Electrospray Ionization Coupled with Gas  
366 Chromatography. *Analytical chemistry* **2018**, *90* (6), 4203–4211. 367

(21) van Berkel, G. J.; McLuckey, S. A.; Glish, G. L. Electrochemical  
368 origin of radical cations observed in electrospray ionization mass  
369 spectra. *Anal. Chem.* **1992**, *64* (14), 1586–1593. 370

- 371 (22) Yourdkhani, S.; Chojecki, M.; Korona, T. Substituent effects in  
372 the so-called cation $\pi$  interaction of benzene and its boron-nitrogen  
373 doped analogues: overlooked role of  $\sigma$ -skeleton. *Phys. Chem. Chem.*  
374 *Phys.* **2019**, *21* (12), 6453–6466.
- 375 (23) Ma, J. C.; Dougherty, D. A. The Cation- $\pi$  Interaction. *Chem.*  
376 *Rev.* **1997**, *97* (5), 1303–1324.